

# Cross-pore electrostatic repulsions are critical for stabilizing the GABA<sub>A</sub> receptor open state

Sruthi Murlidaran<sup>a,1</sup>, Reza Salar<sup>a,b,2</sup>, and Grace Brannigan<sup>a,b,3</sup>

<sup>a</sup>Rutgers University, Center for Computational and Integrative Biology, Rutgers University, Camden, NJ, USA; <sup>b</sup>Department of Physics, Rutgers University, Camden, NJ, USA

GABA<sub>A</sub> receptors (GABA<sub>A</sub>R) are critical for proper transmission of inhibitory signals in the central nervous system, and are common targets of anesthetic and anxiolytic drugs. Several naturally occurring mutations in such receptors can cause an increased likelihood of seizures. In particular, gamma-K289M on the M2-M3 loop attached to the pore-lining M2 helices is associated with Generalized Epilepsy and Febrile Seizures. At the single channel level, the mutation dramatically reduces current amplitude in some subspecies, and increases deactivation rate in other subspecies. The molecular mechanism through which the mutation causes these effects is unknown. Using a homology model of the GABA<sub>A</sub>R based on the recently solved structure for the homologous glutamate-gated chloride channel (GluCl), we ran molecular dynamics simulations of multiple replicas incorporating both the Wild-type and the mutation, at room temperature and at temperatures inducing febrile seizures. These simulations have shown distinct effects on conformations and conductance of the channel. From these results we propose a molecular mechanism for rapid but unstable closure of GABA<sub>A</sub>R, which would be likely to cause flickering effect reported by experimental studies, in single channel recordings.

## INTRODUCTION

Pentameric Ligand-gated Ion Channels (pLGICs) are essential components of the post-synaptic membrane, serving both inhibitory and excitatory roles. pLGIC sequence varies significantly within and between prokaryotes and eukaryotes,(1) with typical homologies of about 30%. pLGIC function tends to be quite sensitive to even small differences in sequence, but numerous pLGIC structures have now demonstrated significant structural conservation despite functional variation. This property has made it challenging to isolate the roles of various pLGIC components or sequence variations in subtle functional effects.

Despite the high sequence variation among pLGIC subunits, even for those forming a heteromeric channel, few single nucleotide polymorphisms (SNPs) are found among populations within coding regions for a specific subunit. Mutations causing loss of function in inhibitory receptors or gain of function in excitatory receptors can result in seizures induced by neuron overexcitation. Many naturally occurring mutations are associated with various forms of epilepsy(2–5), with several relevant mutations identified even before the use of genome-wide association studies. The molecular mechanisms underlying the effect of nearly all mutations on signaling are unknown.

GABA is the primary inhibitory neurotransmitter in the central nervous system; inhibition is partially transduced by extracellular binding to the type A GABA receptor, an anionic pLGIC(6–8). Many molecules with sedative, anxiolytic, and anesthetic properties are positive modulators of the GABA<sub>A</sub>R, including neurosteroids(9–13), benzodiazepines(14), and in-

halational and intravenous general anesthetics(15–17). Negative modulators, such as pregnenolone sulfate(18), can induce seizures, as can certain mutations. Seizures associated with inherited mutations typically require conditions that are found only infrequently; survival is unlikely in the presence of consistent seizures. GABA<sub>A</sub>R receptors with these mutations are therefore known a priori to be functional under typical conditions but dysfunctional under well-defined alternate conditions, making them promising candidates for identifying the role of the mutated residue.

Each subunit consists of an extracellular agonist-binding domain (ECD) and a transmembrane domain containing a four helix bundle with helices labeled (M1-M4). The M2 helices line the pore, and the M2-M3 loop connecting the M2 and M3 helices interacts directly with the ECD. The loop has long been hypothesized to “communicate” agonist binding to the transmembrane domain,(19–27) with several mutation studies indicating the importance for agonist sensitivity of short-range attractive electrostatic interactions, such as salt-bridges, between the M2-M3 loop and the ECD. (28–31)

In GABA<sub>A</sub>R subunits the M2-M3 loop contains a basic residue appearing at the homologous positions of  $\alpha$ 279,  $\beta$ 274, or  $\gamma$ 289, denoted as M2 24' in the prime numbering scheme suggested in (1). Harrison and colleagues(30) demonstrated that charge-reversal of  $\alpha$ 279 reduced agonist sensitivity (EC50) which was restorable via additional charge-reversal of  $\alpha$  D57 or  $\alpha$ D149, both within the ECD and expected to be near the M2-M3 loop. Maximum whole-cell current, however, was reduced by about 1/3 upon the single  $\alpha$ D279K mutation, and further reduced by about the same amount with the second mutation of  $\alpha$  D57K or  $\alpha$ D149K, suggesting a significant role for  $\alpha$ 279K in stabilizing the open state beyond forming a salt-bridge with the ECD. Similar behavior was observed in the nicotinic acetylcholine receptor (nAChR), upon charge-reversal of  $\alpha$ R209 in M1 and  $\alpha$  E45 in the ECD.(25)

A natural but uncommonly occurring SNP at the homologous residue in the  $\gamma$  subunit ( $\gamma$ 2 K289), further suggests an additional role for this residue beyond gating, because the  $\gamma$  subunit does not form GABA binding cavities. The  $\gamma$ 2K289M mutation has been reported in families with generalized epilepsy and febrile seizures plus(GEFS+)(2, 32, 33), a generalized phenotype that often includes only febrile (fever-caused) seizures until about age 11, but can also include less severe myoclonic, atonic, or absence seizures at normal body temperature. In  $\alpha_1\beta_2\gamma_2$  K289M receptors, GABA-evoked current amplitude was dramatically reduced relative to the WT (33, 34), while in  $\alpha_1\beta_3\gamma_2$ K289M receptors the mutation did not affect current amplitudes but did increase the deactivation rate(35). In the latter receptors, currents had reduced mean

open times, in part due to flickering(2, 31, 36). In hippocampal neurons containing GABA<sub>AR</sub> with  $\gamma_2$ :K289M subunits accelerated deactivation of inhibitory post synaptic currents was also observed(35).

Little information has been available regarding the effect of the mutation on GABA<sub>AR</sub> structure and dynamics. Using a homology model of the GABA<sub>AR</sub> receptor based on the medium resolution cryo electron microscopy structure of the nicotinic Acetylcholine Receptor (nAChR), Brownian Dynamics Simulations of ion conduction were used to suggest that mutant receptors display reduced conductance due to reduced affinity of the ion for the ion channel(37). However, the recent x-ray structures of eukaryotic and prokaryotic homologs have suggested that alignment of the sequence with the electron density map in the M2 helices is likely incorrect in the structure used for these simulations. Furthermore, these simulations do not contain explicit representations of water or lipid molecules.

The temperature dependence of this mutation suggests a significant role for entropy and conformational fluctuations in determining its effects. Here we conduct molecular dynamics simulations with multiple replicas of the  $\gamma_2$  K289 and M289 forms of the receptor, at both lower and higher temperatures. We observe a moderately narrowed pore in the M289 receptor at 300K, and a significantly narrowed pore at 315K. Through adaptive biasing force (ABF) calculations, we demonstrate that the effects at 315K result in a substantially higher barrier for conduction of a chloride ion.

$\gamma_2$  K289 was not observed to form salt bridges with the ECD, and these conformational effects showed no clear correlation to any salt-bridging pattern. We propose instead that the five conserved basic residues at this position form a ring of positive charge that effectively pushes the five M2-M3 loops away from the center, pulling M2 helices with it, and stabilizing the open state. Neutralizing one of the charges as with  $\gamma_2$ K289M reduces this repulsion. When it is combined with a temperature increase that softens the conformational preferences resulting from remaining interactions common to both K and M receptors, the non-temperature dependent change in electrostatic repulsions dominates.

We present a simple variational theory that quantitatively predicts the effect of  $\gamma_2$ :K289M on the preferred separation of M2-M3 loop charges, using only the mean and standard deviation of the separation in the wild type  $\gamma_2$ :K289 channel. Temperature dependence appears through both the effect of temperature on the standard deviation and as a linear term in the theory. The success of the theory supports a critical role for these electrostatic repulsions in stabilizing the wild-type receptor and also in transducing the effects of the mutation.

## MATERIALS AND METHODS

### Homology Models

A high resolution structure of a GABA<sub>AR</sub> was not available until the recent publication of 3Å resolution structure for a  $\beta_3$  homopentamer. In the transmembrane domain, homology between GABA<sub>AR</sub>  $\alpha$  or  $\gamma$  to GABA<sub>AR</sub>  $\beta$  is not significantly improved relative to homology between GABA<sub>AR</sub>  $\alpha/\gamma$  subunits and GluCl $\alpha$  (need numbers), and as a result homology models of  $\alpha\beta\gamma$ GABA<sub>AR</sub> built on the GABA<sub>AR</sub>  $\beta_3$  homopentamer are not expected to be significantly improved relative to those based on GluCl. The model used in this paper corresponds to Model 1 - CHOL from Reference(38), and was

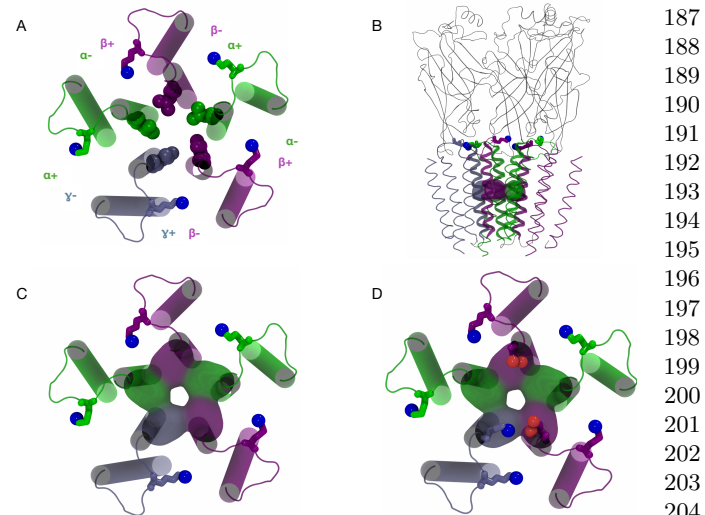


**Fig. 1.** (A) Side View of EC and TM domain showing  $\gamma$  subunit in blue ; (B) View of TM domain, looking down on the membrane from the extracellular region, where each subunit(colored as in A) comprises of a four helix bundle(M1-M4). M1 is gray, M2 is purple, M3 is pink and M4 is ochre; Side view (C) and view from the top-down to (D) the TM domain showing the mutation K289M in the M2-M3 loop and the LEU residues at the 9' location.

built with GluCl (PDB code : 3RHW) as a template as well as the alignments published in Ref(39). Further justification and details on this model can be found in Reference(38)

**System Setup.** This manuscript considers data from four simulations at 300K and four simulations at 315K, with 2 wild type (termed K1, K2) and 2 mutant (M1, M2). The systems were prepared as in Ref(38), by embedding the protein in a lipid bilayer composed of 4:1 phosphatidylcholine (POPC) : cholesterol mixture built using CHARMM Membrane builder, with the final system containing 268 POPC and 71 membrane CHOL molecules. In addition to membrane cholesterol, this model includes cholesterol docked to five pseudo-symmetric intersubunit sites, with implications and justification for this decision reported in (38). The systems were solvated using the SOLVATE plugin in VMD(40) and neutralizing ions were added to bring the system to a 0.15M salt concentration using the AUTOIONIZE plugin. The final system contained about 160,000 atoms.

**Simulation Methods.** All simulations used the CHARMM22-CMAP(41) force field with torsional corrections for proteins. The CHARMM36 model(42, 43) was used for phospholipids, ions, water and cholesterol molecules. Energy minimization and MD simulations were conducted using the NAMD2.9 package(44). All simulations employed periodic boundary conditions, long-ranged electrostatics were handled with smooth particle mesh Ewald method, and a cutoff of 1.2 nm was used for Lennard-Jones potentials with a switching function starting at 1.0 nm. All simulations were run in the NPT ensemble with weak coupling to Langevin thermostat and a barostat at a respective 300 K/315 K and 1 atm. All bonds to the hydrogen atoms were constrained using the SHAKE/RATTLE algorithm. A multiple time-step rRESPA method was used, and controlled with a high frequency time-step of 2fs and low frequency time-step of 4fs. All the systems were energy minimized for 10000 steps, then simulated for 5 ns with restraints

249 of 1 kcal/mol/Å applied to the  $C_\alpha$  atoms of the protein. Restraints were then removed and 195 ns of nearly unrestrained simulation was carried out in all four systems. During this period of the simulation, only harmonic restraints (force constant 0.4 kcal/mol/Å) between the intracellular ends of the M3 and M4 helices were used, to mimic the effects of the intracellular domain and prevent separation of the M4 helix from the rest of the bundle. High temperature (315K) simulations were run for 500 ns following the 200 ns simulations at lower temperature (300K).

259 *Conformational Analysis:* Measurement and analysis of the 260 pore radii has been carried out using the HOLE software (45) 261 and TCL scripting through VMD(40). Python scripts have 262 been used to analyze and visualize the hydration of the pore 263 throughout the simulation.

264 *Poisson-Boltzmann Calculations:* The Poisson-Boltzmann 265 (PB) profile for conduction of both a  $\text{Na}^+$  and  $\text{Cl}^-$  through 266 the ion channel was calculated using APBSmem(46). The pre- 267 generated PQR format of the proteins using PDB2PQR(47) 268 tool was used as the input for the electrostatic potential cal- 269 culations. These calculations were performed for initial non- 270 equilibrated structures of the protein, as well as for conforma- 271 tions extracted from the last 50 ns of both the 300K and 315K 272 MD simulations (for  $\text{Cl}^-$ ).

273 *SMD Simulations:* Steered Molecular Dynamics (SMD) 274 simulations (48, 49) were used to obtain favorable positions of 275 the ion at different positions along the channel, for later use 276 in Adaptive Biasing Force (ABF) calculations. The chloride 277 ion was pulled along the pore of the channel at a constant 278 velocity of 10 Å/ns. The force required to pull at constant 279 velocity is also calculated, and can, in principle, be used to 280 calculate a potential of mean force (PMF) using Jarzynski's 281 equation (50, 51), but in practice it is rarely possible to achieve 282 a sufficiently slow pulling speed.

283 *ABF Simulations:* Adaptive biasing force calculations 284 (ABF)(52–55) were used to measure the PMF (free energy 285 profile) of a chloride ion translocating the GABA<sub>A</sub>R ion chan- 286 nel at 315K, for both the WT and K289M channels. ABF 287 was performed using the Collective Variables module(56) of 288 NAMD2.9. The pore axis was divided into 23 bins of each 289 5 Å length. Initial coordinates for the ion were obtained from 290 SMD simulations. One thousand samples were collected in 291 each bin prior to the application of ABF to avoid undesired 292 non-equilibrium effects on the dynamics. Fifteen ns of trajec- 293 tory were generated in most bins, while bins near the primary 294 barrier in the pore contained 25 ns.

## 297 1. THEORY

298 The ring of five basic residues can be approximated as five 299 positive charges arranged in a pentamer, each a distance  $r$  from 300 the center, which we refer to as the +5 ring. The thermally 301 excited ring may “breathe”, causing  $r$  to fluctuate, but for 302 simplicity all charges are treated as equidistant from the center. 303 The variation in  $r$  is given by the time-average

$$305 \quad \delta r^2 = \langle (r(t) - \bar{r})^2 \rangle. \quad [1]$$

307 At equilibrium, the wild-type receptor exhibits normal fluctua- 308 tions of  $r$  around its time average  $\bar{r}$ . The free energy of the 309 wild-type receptor as a function of the +5 ring radius  $r$  can

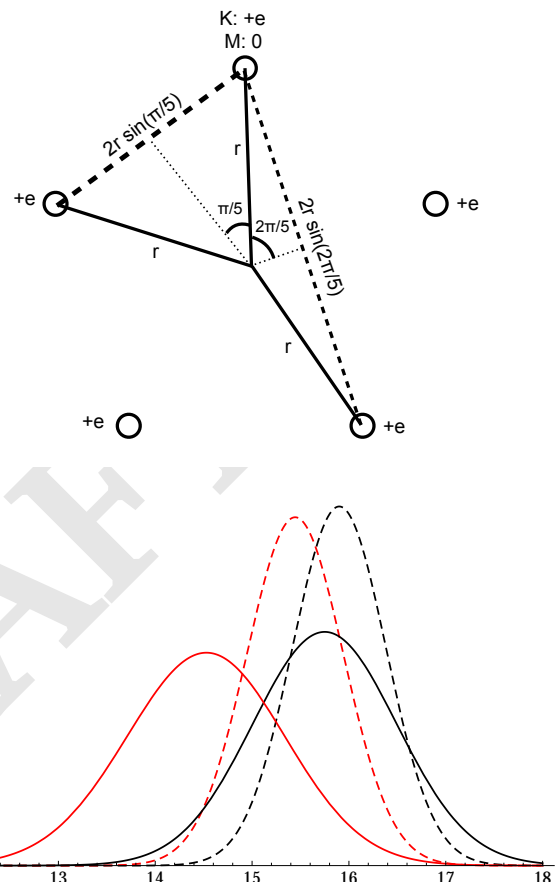


Fig. 2. A) A conserved basic residue in the M2-M3 loop yields a pentamer of (unscreened) positive charges, which we refer to as the +5 ring, corresponding to  $\gamma$  K289,  $\alpha$  K279, or  $\beta$  K274. The total energy of the +5 ring increases as the ring closes (and  $r$  gets smaller), reducing/increasing the distance/repulsion between like-charges. The  $\gamma$  K289M mutation neutralizes one of the charges, yielding a +4 ring, which can shrink with a lowered energetic cost. B) (Placeholder) Predicted distribution of  $r$  generated using values in Table 1; black is for a +5 ring (as in K289) while red is for a +4 ring (as in M289); dashed lines are for 300K and solid lines for 315 K.

373 be expanded harmonically as

$$375 \quad H_K(r) = \frac{k_r(r - \bar{r}_K)^2}{2\bar{r}_K}, \quad [2]$$

378 where the time-average of  $r$  is noted by  $\bar{r}_K$ , and  $k_r$  is the  
379 temperature-dependent coefficient governing fluctuations:

$$381 \quad k_r = \frac{RT \bar{r}_K}{\langle (r - \bar{r}_K)^2 \rangle}, \quad [3]$$

384 where  $R$  is the gas constant and  $T$  is the temperature.

385 The mutation  $\gamma$ K289M removes the four long-range repulsive  
386 electrostatic interactions involving  $\gamma$ K289. Shrinking the  
387 pentameric ring is therefore less unfavorable in the presence of  
388 the mutation, and the free energy as a function of  $r$  is reduced  
389 by the Coulomb energy of the lost interactions:

$$391 \quad \Delta U(r) = \frac{-k_e e^2}{r} \left( \frac{1}{\sin 2\pi/5} + \frac{1}{\sin \pi/5} \right) = -\frac{ck_e e^2}{r} \quad [4]$$

394 where  $c \sim 2.75$ ,  $e$  is the electron charge, and  $k_e =$   
395  $332\text{\AA}/\text{kcal/mol}/e^2$  is the Coulomb constant. Note that this  
396 simplification is reasonable primarily because all five charges  
397 are nearly coplanar in a plane perpendicular to the pore axis.  
398 Other electrostatic interactions will also be lost, but it is rea-  
399 sonable to neglect them because they involve residues screened  
400 by another oppositely charged residue, and/or they do not  
401 have a significant radial component. The total free energy for  
402 the mutant receptor is therefore

$$404 \quad H_M(r) = H_K(r) + \Delta U(r) \quad [5]$$

$$405 \quad = \frac{k_r(r - \bar{r}_K)^2}{2\bar{r}_K} - \frac{ck_e e^2}{r} \quad [6]$$

$$406 \quad = k_r \bar{r}_K \left( \frac{(r - \bar{r}_K)^2}{2\bar{r}_K^2} - \frac{\kappa \bar{r}_K}{r} \right), \quad [7]$$

407 where

$$412 \quad \kappa \equiv \frac{c k_e e^2}{k_r \bar{r}_K^2} = \frac{c}{RT} \frac{k_e e^2}{\bar{r}_K} \frac{\delta r^2}{\bar{r}_K^2} \quad [8]$$

413 The average radius for the mutant receptor,  $\bar{r}_M$ , minimizes  
414  $H_M$ :

$$417 \quad \left. \frac{\partial H_M(r)}{\partial r} \right|_{\bar{r}_M} = k_r \left( 1 - \frac{\bar{r}_M}{\bar{r}_K} - \kappa \left( \frac{\bar{r}_K}{\bar{r}_M} \right)^2 \right) = 0. \quad [9]$$

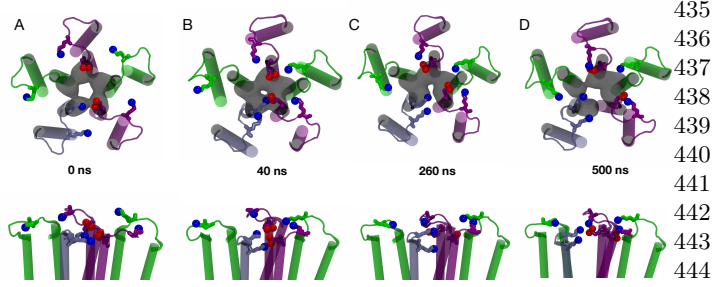
420 Defining the ratio between the two mean radii  $\alpha \equiv \bar{r}_M/\bar{r}_K$ ,  
421 Equation 9 reduces to  $1 - \alpha - \kappa/\alpha^2 = 0$ . This equation has  
422 an exact, real solution for  $\kappa < 4/27$  ( $\frac{k_e e^2}{k_r \bar{r}_K^2} < 0.035$ ), which  
423 when expanded around  $\kappa = 0$  is

$$426 \quad \alpha = \frac{\bar{r}_M}{\bar{r}_K} = 1 - \kappa - 2\kappa^2 - 7\kappa^3 + O(\kappa^4). \quad [10]$$

428 To first order in  $\kappa$ , we predict that

$$431 \quad \bar{r}_M = \bar{r}_K - \frac{ck_e e^2}{RT} \frac{\delta r^2}{\bar{r}_K^2} \quad [11]$$

434 where  $ck_e e^2/R = 8.3 \times 10^5 \text{ \AA K}$ .



435  
436  
437  
438  
439  
440  
441  
442  
443  
444  
445  
446  
447  
448  
449  
450  
451  
452  
453  
454  
455  
456  
457  
458  
459  
460  
461  
462  
463  
464  
465  
466  
467  
468  
469  
470  
471  
472  
473  
474  
475  
476  
477  
478  
479  
480  
481  
482  
483  
484  
485  
486  
487  
488  
489  
490  
491  
492  
493  
494  
495  
496

Fig. 3. Snapshots of the channel, view from the ECD and side view, at different time-frames, depicting the chain of events leading to the opening of the channel.

## RESULTS AND DISCUSSION

**Significant effect of cross pore repulsion..** For comparison with the analytical model of the +5 ring presented in Theory, the mean  $\bar{r}_K$  and standard deviation  $\sqrt{\delta r_K^2}$  of the distance of +5 ring charges from the pore axis (see Figure 2) were measured for the WT systems at each temperature. Results are in Table 1, showing that  $\bar{r}_K$  was not sensitive to temperature, while  $\sqrt{\delta r_K^2}$  increased with temperature, as expected. These values, as well as Equations 3 and 8, were used to calculate the parameters  $k_R$  and  $\kappa$  for each temperature.

Eq. 11 was used to generate predictions for  $\bar{r}_M$ , which were reduced relative to  $\bar{r}_K$  at both temperatures, but with a much larger reduction at higher temperatures. Quantitative agreement was very good, especially given the simplicity of the theory; at 300K we predicted a 3.1% reduction upon mutation, but obtained a reduction of 2.5%, while at 315K we predicted an 8.2% reduction but obtained a 6.3% reduction. In both cases, the reduction was overestimated, which may reflect computational limits on equilibration time for the K289M receptor, or a higher order contribution to  $H_K(r)$  resulting in a steeper free energy cost when  $r - \bar{r}_K$  is large.

Table 1. Observed values and extracted parameters from analysis of +5 ring in WT receptors, and predicted and observed values upon mutating K289M (yielding +4 ring).

$T(K)$	$\bar{r}_K(\text{\AA})$	$\bar{r}_M(\text{pred. \AA})$	$\bar{r}_M(\text{obs. \AA})$	$\sqrt{\delta r_K^2}(\text{\AA})$	$\kappa$	$k_R/\bar{r}_K(\text{kcal/mol/\AA}^2)$
300	15.9	15.4	15.5	0.27	0.027	8.5
315	15.8	14.5	14.8	0.42	0.066	3.6

Although the simple electrostatic effects of neutralizing one charge in the +5 ring predict the observed closing of that ring, a functional effect requires that radius of the +5 ring is coupled to some changes in the dynamics of the protein that results in changes in radius of the pore.

**Spontaneous opening event at 315 K.** In one of the WT systems, simulation starts with  $\alpha$ -K279 side-chain facing away from the pore as shown in Figure 3 A. As the simulation progresses, there occurs a chain of events that results in the opening of the channel. Proximity of residues  $\gamma$ -K285 and  $\beta$ -E270 results in the formation of a salt-bridge between them (Figure 3 B). This salt-bridge is, however unstable, due to residue  $\beta$ -K274 hovering near  $\beta$ -E270. As the residue  $\alpha$ -K279

497  
498  
499  
500  
501  
502  
503  
504  
505  
506  
507  
508  
509  
510  
511  
512  
513  
514  
515  
516  
517

518 faces towards the pore (Figure 3C), this causes the residue  
519  $\gamma$ -K285 to face downward to mitigate the repulsive force thus  
520 completely breaking the salt-bridge with  $\beta$ -E270 (Figure 3C).  
521 This allows  $\beta$ -E270 to salt-bridge more stably with  $\beta$ -K274  
522 (Figure 3D). Similar  $\beta$ -270-274 salt-bridge is formed through-  
523 out the simulation on the other  $\beta$  subunit. The synchronized  
524 formation of both the salt-bridges, allows pore subunits to  
525 separate from each other thus opening the pore. To play-out  
526 sequence of events in an explicit manner, the time of the events  
527 are plotted as shown in Figure 4. At around 260-280 ns, we  
528 see that the  $\alpha$ -K279 side-chain flips (Figure 4B; green curve),  
529 more stable formation of the SBs,  $\beta$ -270-274 on both the  $\beta$   
530 subunits (Figure 4A; red, maroon curve). These events are  
531 also coupled with the LEU-gate backbone atoms moving away  
532 from each other (Figure 4B; Black curve), thus opening the  
533 pore. Another simultaneous event that triggers the formation  
534 of the key salt-bridges is the unfavorable proximity of the E270  
535 residue of both the  $\beta$  subunits (Figure 5 B; curve Blue). When  
536 these residues do not form the SB with their respective  $\beta$   
537 -K274 partners (Figure 5 B; curve Black, thick and dashed  
538 lines), this brings the E270 residues face each other in the  
539 pore, thus causing an unfavorable repulsion which initiates  
540 the pore opening process (Figure 5 B; curve Green). Position  
541 of these residues are as depicted in the network diagram as  
542 shown in (Figure 5 A).

543  
544 **Pore-radii distribution based on SB.** To further validate the  
545 opening of pore when both SBs are formed, the distribution of  
546 pore radii based on the formation of SB was calculated. This  
547 finding showed that, when both SB's were formed, there was  
548 more probability of finding the channel in an open confor-  
549 mation (Figure 6).

550  
551 **Effects of Mutation on SB formation and pore radii.** The pore  
552 radius profile (averaged across two replicas) for the K289M and  
553 WT receptors is shown in Figure 7. The minimum constriction  
554 region (flanked by hydrophobic leucine residues) occurs at  
555 roughly the same height along the pore axis for the two systems,  
556 but is substantially tighter for the averaged mutant structure,  
557 particularly at higher temperatures.

558 As shown in Figure 8, overlap between K289M and WT

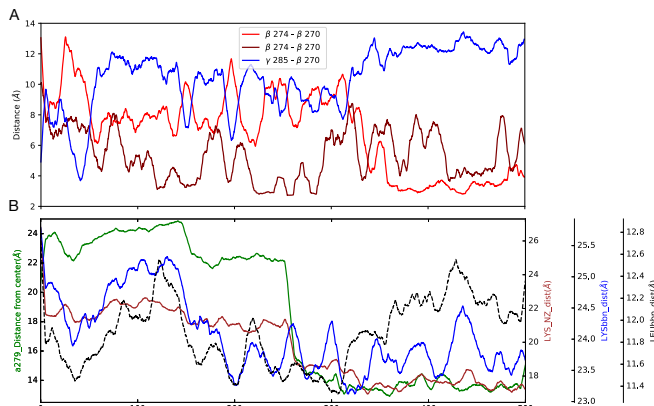


Fig. 4. yet to be written

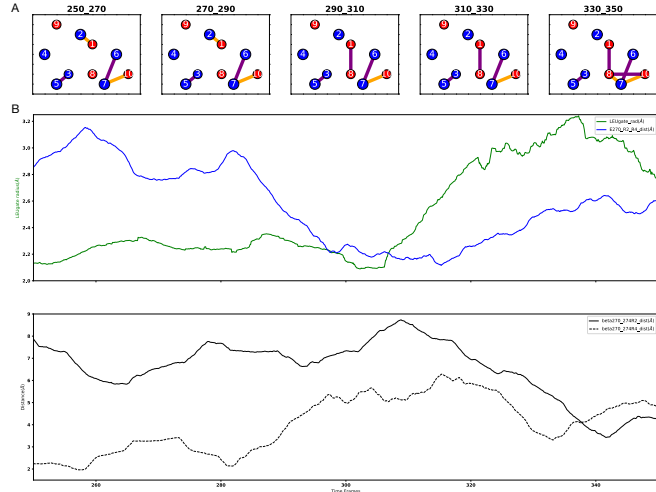


Fig. 5. (A). Network diagram, depicting the position of the residues involved in opening of the channel. Colored by charge.(1,8-  $\beta$ -E270; 2,7-  $\beta$ -K274; 4,6-  $\alpha$ -K279; 5-  $\gamma$ -K289, 3-  $\gamma$ -K285; 9,10-  $\alpha$ -D55. (B).Distance between both the  $\beta$ -E270 residues(blue) and the Leusine-gate radius(green) variation with respect to the time frames(250-350ns);

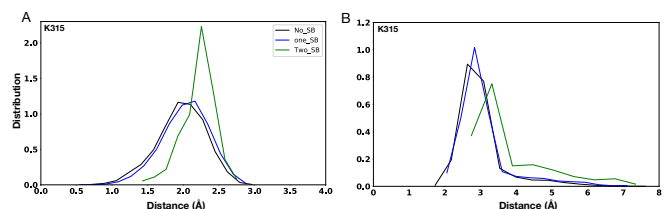
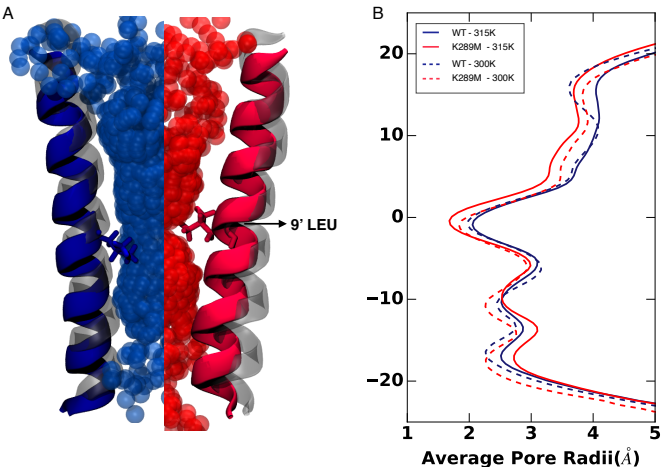
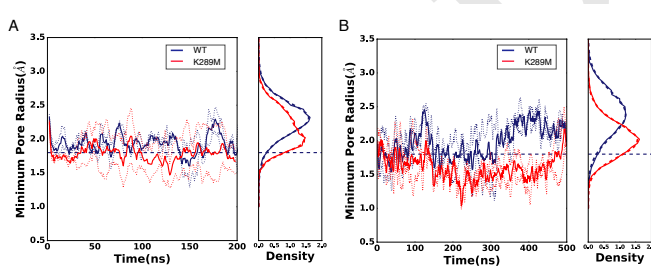


Fig. 6. (A). Pore radii distribution based on the formation of the  $\beta$ -K274-E270 salt-bridges. Green curve denotes the frames when both the SBs are formed. Blue and Black curves denote the frames at which one and no SBs are formed, respectively.



**Fig. 7.** (A) Space-filling models computed from simulations at 315 K, depicting the reduced pore radii of the K289M (red) as compared to that of the WT (blue). (B) Radii of the transmembrane domain along the Z-axis, averaged over all the frames. The pore profile around the 9' region is more constricted at the higher temperature when compared to that of the lower temperature, in both the WT and the K289M. The space filling models further compares the significant reduction in the pore radius in the K289M to the fairly open WT, and the movement of helices compared to their respective initial conformations(grey).



**Fig. 8.** Smoothed time evolution of the pore minimum constriction, averaged (solid lines) over two replicas (dotted lines) each, at 300 K(A) and 315 K(B). The minimum constriction, formed around the 9' region is visibly more constricted for the K289M systems and this reduction is more pronounced at higher temperature. The minimum constriction region in K289M falls below the chloride ion radius of 1.8 Å, thus driving it to a closed state. The probability distribution further shows a clear shift in the peak of the K289M systems towards reduced pore radii at a higher temperature.

trajectories (including individual replicas) is substantial at 300K, although the distribution of minimum pore radii is shifted slightly downward (smaller) for the mutant receptor. At 315K, this overlap is substantially reduced, with both WT replicas yielding conformations with persistently larger pore radii than both K289M replicas. These trends mimic those observed in the +5 ring.

Determining whether a single conformation corresponds to an “open” or “closed” state is not typically possible in MD simulations, but we note here that a Cl- atom has a radius of approximately 1.8 Å; at 300K, the minimum pore radius is greater than 1.8 Å for 69% (WT) and 43% (K289M) of the frames, while at 315K, the minimum pore radius is greater than 1.8 Å for 69% (WT) and 26% (K289M) of the frames.

All simulations here were done in the absence of GABA or other agonist, which is not stable in the agonist-binding site due to limitations of classical non-polarizable forcefields for capturing cation-π interactions. The presence of agonist would likely alter  $\bar{r}_K$  and/or  $k_R$ , but would not affect  $\Delta U(r)$ , which depends only on protein sequence.

The effects of the mutation on purely electrostatic barriers for chloride ion translocation was quantified via the Poisson-Boltzmann equation as described in Methods. The mutation from a positively charged to neutral residue led to minute changes in the electrostatic profile given identical initial structures (as shown in Supplementary Figure S2(A) and Figure S2(B)), suggesting that the mutation alone could not affect conductance without any conformational changes.

The calculation performed on equilibrated structures of WT and K289M receptors showed a 5–10 kcal/mol (Figure S2(C)) higher electrostatic barrier in K289M, predominantly occurring in the transmembrane domain enclosing the residues containing the minimum pore constriction region. The LEU-gate constriction in addition to the loss of long range electrostatic interactions from K289 seems to contribute to the formation of higher barrier in the K289M. We note that these calculations includes electrostatic contributions, but not van der Waals or entropic contributions; these terms are included in the measurement of the potential of mean force via Adaptive Biasing Force calculations as described subsequently.

The PMF for chloride ion translocation at 315K, measured using ABF, is shown in Figure 9. The largest barrier occurs more proximal to the leucine residues forming the tightest constriction; this barrier is increased by 5 kcal/mol for the mutant receptors. A slight, broad well (relative to a reference position outside the receptor) is apparent around residue 289 in the PMF for the WT receptor, while at the same location in the K289M receptor the PMF is slightly elevated relative to the reference location. However, these differences are slight compared to the effects of the mutation on the primary barrier, indicating that while mutation of a positively charged to neutral residue does have a small effect on affinity of the chloride ion for the region of the receptor near the mutation, the dominant effect of the mutation on conduction is via conformational instability of the open state.

## CONCLUSION

Proteins that require ligand-induced conformational change have an inherent design challenge. Free energy differences between conformations must change sign upon ligand binding, constraining the magnitude of this free energy difference in

745  
746  
747  
748  
749  
750  
751  
752  
753  
754  
755  
756  
757  
758  
759  
760  
761  
762  
763  
764  
765  
766  
767  
768  
769  
770  
771  
772  
773  
774  
775  
776  
777  
778  
779  
780  
781  
782  
783  
784  
785  
786  
787  
788  
789  
790  
791  
792  
793  
794  
795  
796  
797  
798  
799  
800  
801  
802  
803  
804  
805  
806

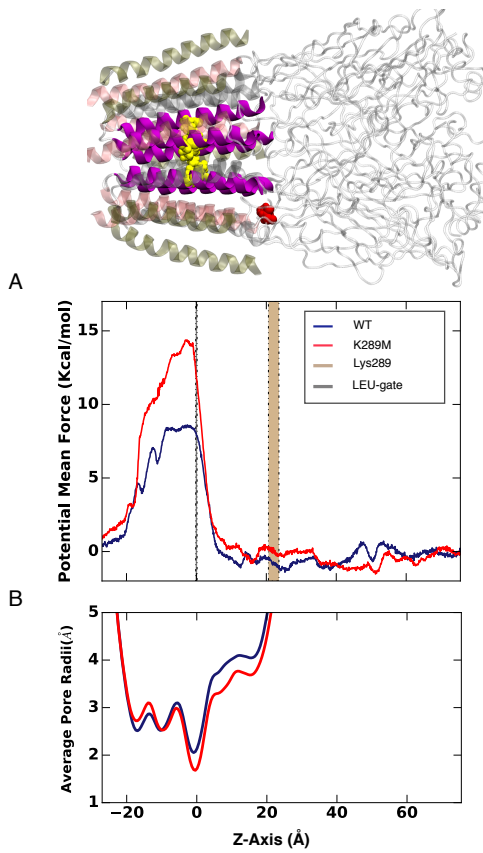


**Fig. 9.** Potential of mean force profile of chloride ion transport (A) Aligned below the horizontally laid protein figure is the plot showing the potential mean force experienced by the ion as it moves through the channel along the Z-axis. (B) These barriers in the channel are further compared with the average pore radius of the TM region of the channel. These comparisons clearly explains that the highest barriers are found at the 9' regions which forms the minimum constriction region. The difference between the barriers at this region is approximately 5 Kcal/mol.

either the bound or apo state. This behavior must still be robust to temperature variations experienced within the organism. Although that temperature range is relatively narrow for endothermic animals, it includes elevated temperatures for fighting infection. Differences in body temperature among endothermic species may also drive some sequence differences in non-metabolic proteins.

In this work, we investigated the effects of a fever-associated charged-to-hydrophobic mutation in a human ligand-gated ion channel, allowing us to identify the significance of collective, long-range, electrostatic interactions for maintaining the protein's function at higher temperatures. The temperature-dependent structural effect of reducing these electrostatic interactions via substitution of K to M at  $\gamma 2$ : M2 24' can be well-predicted simply by considering Coulombic repulsions between charged residues at M2 24' in all subunits, as well as a simple variational theory which introduces temperature effects. The phenomenon of unstable activation in  $\gamma 2$  K289M GABA<sub>A</sub>R, previously observed *in vivo* and *in vitro*, has now been observed *in silico* and *in principio*.

A basic residue at 24' in the M2-M3 loop is highly conserved across GABA<sub>A</sub>R subunits, but not across all pLGICs. It is not necessary, however, that charged residues be positioned at 24' for cross-pore repulsions to stabilize open conformations, but simply that they be in the same position in each subunit. Crucial collective interactions might therefore be well indicated by the presence of a charged residue that appears at the same position in all pore-sharing species (i.e. all GABA<sub>A</sub>R subunits or all GlyR subunits), but which is non-conserved across pLGICs in general.

To maintain the necessary range for cross-pore interactions, it is critical that the charged residues be unscreened. Presence of a nearby oppositely charged residue in one subunit will reduce the charge-charge interaction ( $1/r$ ) to a charge-dipole interaction ( $1/r^2$ ), with presence of an additional charged residue on the other side yielding a dipole-dipole interaction ( $1/r^3$ ). Screening may be affected by changes in pH as well as participation in salt-bridges, suggesting a mechanism that may be crucial for gating in numerous other pLGICs. Based on these results and those in Ref. (30), we suggest that  $\alpha$ D57 or  $\alpha$ D14 may screen  $\alpha$ K279 (M2 24') in the apo state, while binding of GABA changes conformation of  $\alpha$ D57 or  $\alpha$ D14, leaving  $\alpha$ K279 (M2 24') unscreened, increasing cross-pore repulsions among positively charged residues at M2 24', and opening the pore.

## SUPPLEMENTARY MATERIAL

869	931
870	932
871	933
872	934
873	935
874	936
875	937
876	938
877	939
878	940
879	941
880	942
881	943
882	944
883	945
884	946
885	947
886	948
887	949
888	950
889	951
890	952
891	953
892	954
893	955
894	956
895	957
896	958
897	959
898	960
899	961
900	962
901	963
902	964
903	965
904	966
905	967
906	968
907	969
908	970
909	971
910	972
911	973
912	974
913	975
914	976
915	977
916	978
917	979
918	980
919	981
920	982
921	983
922	984
923	985
924	986
925	987
926	988
927	989
928	990
929	991
930	992

- 993 1. Jaiteh M, Taly A, Hénin J (2016) Evolution of pentameric ligand-gated ion channels: Pro-loop  
994 receptors. *PLoS one* 11(3):e0151934.  
995 2. Bianchi M, Song L (2002) Two different mechanisms of disinhibition produced by GABA<sub>A</sub>  
996 receptor mutations linked to epilepsy in humans. *The Journal of ...* 22(13):5321–5327.  
997 3. Cossette P, et al. (2002) Mutation of GABRA1 in an autosomal dominant form of juvenile  
998 myoclonic epilepsy. *Nature genetics* 31(2):184–9.  
999 4. Kang JQ, Kang J, Macdonald RL (2004) The GABA<sub>A</sub> receptor gamma2 subunit R43Q  
1000 mutation linked to childhood absence epilepsy and febrile seizures causes retention of alpha1beta2gamma2S receptors in the endoplasmic reticulum. *The Journal of neuroscience : the official journal of the Society for Neuroscience* 24(40):8672–7.  
1001 5. Macdonald RL, Gallagher MJ, Feng HJ, Kang J (2004) GABA(A) receptor epilepsy mutations. *Biochemical pharmacology* 68(8):1497–506.  
1002 6. Olsen RW, Tobin AJ (1990) Molecular biology of GABA<sub>A</sub> receptors. *FASEB J* 4(5):1469–  
1003 1480.  
1004 7. Macdonald RL, Olsen RW (1994) GABA<sub>A</sub> receptor channels. *Annu Rev Neurosci* 17:569–  
1005 602.  
1006 8. Rabow LE, Russek SJ, Farb DH (1995) From ion currents to genomic analysis: recent advances in GABA<sub>A</sub> receptor research. *Synapse* 21(3):189–274.  
1007 9. Mihic SJ, et al. (1997) Sites of alcohol and volatile anaesthetic action on GABA(A) and glycine  
1008 receptors. *Nature* 389(6649):385–389.  
1009 10. Belelli D, Lambert JJ (2005) Neurosteroids: endogenous regulators of the (GABA(A)) receptor. *Nat Rev Neurosci* 6(7):565–575.  
1010 11. Mitchell EA, Herd MB, Gunn BG, Lambert JJ, Belelli D (2008) Neurosteroid modulation of  
1011 GABA<sub>A</sub> receptors: molecular determinants and significance in health and disease. *Neurochem Int* 52(4–5):588–595.  
1012 12. Lambert JJ, Cooper MA, Simmons RDJ, Weir CJ, Belelli D (2009) Neurosteroids: endogenous allosteric modulators of GABA(A) receptors. *Psychoneuroendocrinology* 34 Suppl  
1013 1: S48—S58.  
1014 13. Olsen RW, Li GD (2011) GABA(A) receptors as molecular targets of general anaesthetics:  
1015 identification of binding sites provides clues to allosteric modulation. *Canadian journal of anaesthesia = Journal canadien d'anesthésie* 58(2):206–15.  
1016 14. Sigel E (1997) The benzodiazepine binding site of GABA<sub>A</sub> receptors. *Trends in Pharmacological Sciences* 18(11):425–429.  
1017 15. Krasowski MD, Harrison NL (1999) General anaesthetic actions on ligand-gated ion channels. *Cell. Mol. Life Sci.* 55(10):1278–1303.  
1018 16. Harris RA, Mihic SJ, Dildy-Mayfield JE, Machu TK (1995) Actions of anaesthetics on ligand-gated ion channels: role of receptor subunit composition. *FASEB J* 9(14):1454–1462.  
1019 17. Miller KW (2002) The nature of sites of general anaesthetic action. *Br. J. Anaesth.* 89(1):17–  
1020 31.  
1021 18. Majewska MD, Mienville JM, Vicini S (1988) Neurosteroid pregnenolone sulfate antagonizes  
1022 electrophysiological responses to GABA in neurons. *Neuroscience Letters* 90(3):279–284.  
1023 19. Campos-Caro A, et al. (1996) A single residue in the M2–M3 loop is a major determinant  
1024 of coupling between binding and gating in neuronal nicotinic receptors. *Proceedings of the National Academy of Sciences of the United States of America* 93(12):6118–23.  
1025 20. Lynch JW, et al. (1997) Identification of intracellular and extracellular domains mediating  
1026 signal transduction in the inhibitory glycine receptor chloride channel. *The EMBO journal*  
1027 16(1):10–20.  
1028 21. Grosman C, Salamone FN, Sine SM, Auerbach A (2000) The extracellular linker of muscle  
1029 acetylcholine receptor channels is a gating control element. *The Journal of general physiology* 116(3):327–40.  
1030 22. Bera AK, Chatav M, Akabas MH (2002) GABA(A) receptor M2–M3 loop secondary structure  
1031 and changes in accessibility during channel gating. *The Journal of biological chemistry* 277(45):43002–10.  
1032 23. Lummis SCR, et al. (2005) Cis-trans isomerization at a proline opens the pore of a  
1033 neurotransmitter-gated ion channel. *Nature* 438(7065):248–52.  
1034 24. Law RJ, Henchman RH, McCammon JA (2005) A gating mechanism proposed from a simulation  
1035 of a human  $\alpha 7$  nicotinic acetylcholine receptor. *Proc. Natl. Acad. Sci. USA* 102(19):6813–  
6818.  
1036 25. Lee WY, Sine SM (2005) Principal pathway coupling agonist binding to channel gating in  
1037 nicotinic receptors. *Nature* 438(7065):243–7.  
1038 26. Unwin N (2005) Refined structure of the nicotinic acetylcholine receptor at 4 $\text{\AA}$  resolution. *J. Mol. Biol.* 346(4):967–989.  
1039 27. Lee WY, Free CR, Sine SM (2009) Binding to gating transduction in nicotinic receptors: Cys-loop  
1040 energetically couples to pre-M1 and M2–M3 regions. *The Journal of neuroscience : the official journal of the Society for Neuroscience* 29(10):3189–99.  
1041 28. Sigel, ErwinBuhr, AndreasBaur R (1999) Role of the Conserved Lysine Residue in the Middle  
1042 of the Predicted Extracellular Loop Between M2 and M3 in the GABA A Receptor. *Journal of Neurochemistry*. Oct99 73(4).  
1043 29. O'Shea SM, Harrison NL (2000) Arg-274 and Leu-277 of the gamma-aminobutyric acid type  
1044 A receptor alpha 2 subunit define agonist efficacy and potency. *The Journal of biological  
1045 chemistry* 275(30):22764–8.  
1046 30. Kash TL, Jenkins A, Kelley JC, Trudell JR, Harrison NL (2003) Coupling of agonist binding to  
1047 channel gating in the GABA(A) receptor. *Nature* 421(6920):272–5.  
1048 31. Hales TG, et al. (2006) An asymmetric contribution to gamma-aminobutyric acid type A receptor  
1049 function of a conserved lysine within TM2-3 of alpha1, beta2, and gamma2 subunits. *The Journal of biological  
1050 chemistry* 281(25):17034–43.  
1051 32. Macdonald R (2010) Mutations in GABA<sub>A</sub> receptor subunits associated with genetic epilepsies. *The Journal of physiology*.  
1052 33. Baulac S, et al. (2001) First genetic evidence of GABA(A) receptor dysfunction in epilepsy: a  
1053 mutation in the gamma2-subunit gene. *Nature genetics* 28(1):46–8.  
1054 34. Ramakrishnan L, Hess GP (2004) On the mechanism of a mutated and abnormally functioning  
1055 gamma-aminobutyric acid (A) receptor linked to epilepsy. *Biochemistry* 43(23):7534–40.  
1056 35. Eugène E, et al. (2007) GABA(A) receptor gamma 2 subunit mutations linked to human epileptic  
1057 syndromes differentially affect phasic and tonic inhibition. *The Journal of neuroscience : the official journal of the Society for Neuroscience* 27(51):14108–16.  
1058 36. Macdonald RL, Kang JQ, Gallagher MJ, Feng HJ (2006) GABA(A) receptor mutations associated  
1059 with generalized epilepsies. *Adv Pharmacol* 54:147–169.  
1060 37. O'Mara M, Cromer B, Parker M, Chung SH (2005) Homology model of the GABA<sub>A</sub> receptor  
1061 examined using Brownian dynamics. *Biophysical journal* 88(5):3286–99.  
1062 38. Hénin J, Salari R, Murlidaran S, Brannigan G, Biology I (2014) A predicted binding site for  
1063 cholesterol on the GABA<sub>A</sub> receptor. *Biophysical journal* 106(9):1938–49.  
1064 39. Hibbs RE, Gouaux E (2011) Principles of activation and permeation in an anion-selective  
1065 Cys-loop receptor. *Nature* 474(7349):54–60.  
1066 40. Humphrey W, Dalke A, Schulter K (1996) VMD: visual molecular dynamics. *Journal of molecular graphics* 14(1):33–8, 27–8.  
1067 41. Mackerell AD, et al. (1998) All-atom empirical potential for molecular modeling and dynamics  
1068 studies of proteins. *The journal of physical chemistry. B* 102(18):3586–616.  
1069 42. Klauda JB, et al. (2010) Update of the CHARMM all-atom additive force field for lipids: validation  
1070 on six lipid types. *The journal of physical chemistry. B* 114(23):7830–43.  
1071 43. Pitman MC, Suits F, Mackellar AD, Feller SE (2004) Molecular-level organization of saturated and  
1072 polyunsaturated fatty acids in a phosphatidylcholine bilayer containing cholesterol. *Biochemistry* 43(49):15318–28.  
1073 44. Phillips JC, et al. (2005) Scalable molecular dynamics with NAMD. *Journal of computational  
1074 chemistry* 26(16):1781–802.  
1075 45. Smart OS, Neduvelli JG, Wang X, Wallace BA, Sansom MS (1996) HOLE: a program for the  
1076 analysis of the pore dimensions of ion channel structural models. *J Mol Graph* 14(6):354–  
1077 360,376.  
1078 46. Callenberg KM, et al. (2010) APBSmem: A graphical interface for electrostatic calculations at  
1079 the membrane. *PLoS ONE* 5(9).  
1080 47. Dolinsky TJ, et al. (2007) PDB2PQR: expanding and upgrading automated preparation of  
1081 biomolecular structures for molecular simulations. *Nucleic acids research* 35(Web Server issue):W522–5.  
1082 48. Isralewitz B, Baudry J, Gullingsrud J, Kosztin D, Schulter K (2001) Steered molecular dynamics  
1083 investigations of protein function. *Journal of Molecular Graphics and Modelling* 19(00):13–  
1084 25.  
1085 49. Park S, Schulter K (2004) Calculating potentials of mean force from steered molecular dynamics  
1086 simulations. *Journal of Chemical Physics* 120(2004):5946–5961.  
1087 50. Jarzynski C (1997) Nonequilibrium Equality for Free Energy Differences. *Physical Review Letters* 78(14):2690–2693.  
1088 51. Jarzynski C (1997) Equilibrium free-energy differences from nonequilibrium measurements:  
1089 A master-equation approach. *Physical Review E* 56(5):5018–5035.  
1090 52. Hénin J, Chipot C (2004) Overcoming free energy barriers using unconstrained molecular  
1091 dynamics simulations. *The Journal of chemical physics* 121(7):2904–14.  
1092 53. Darve E, Rodríguez-Gómez D, Pohorille A (2008) Adaptive biasing force method for scalar  
1093 and vector free energy calculations. *The Journal of chemical physics* 128(14):144120.  
1094 54. Pohorille A, Jarzynski C, Chipot C (2010) Good practices in free-energy calculations. *J Phys  
1095 Chem B* 114(32):10235–10253.  
1096 55. Comer J, et al. (2014) The Adaptive Biasing Force Method: Everything You Always Wanted  
1097 to Know, but Were Afraid to Ask. *The journal of physical chemistry. B*.  
1098 56. Fiorin G, Klein ML, Hénin J (2013) Using collective variables to drive molecular dynamics  
1099 simulations. *Molecular Physics* 111(22–23):3345–3362.  
1100 1101 1102 1103 1104 1105 1106 1107 1108 1109 1110 1111 1112 1113 1114 1115 1116